Quantitative Comparison Against Experiments Reveals Imperfections in Force Fields' Descriptions of Phospholipid–Cholesterol Interactions

Peter Heftberger,[†] Matti Javanainen,[*,‡,¶] Jesper J. Madsen,[§,‖,⊥] Markus S. Miettinen,[#,@,△] O. H. Samuli Ollila,[*,‡,¶] and Georg Pabst[†,∇,††]

†*Biophysics, Institute of Molecular Biosciences, NAWI Graz, University of Graz, 8010 Graz, Austria*

‡*Institute of Organic Chemistry and Biochemistry, Academy of Sciences of the Czech Republic, 16000 Prague 6, Czech Republic*

¶*Institute of Biotechnology, University of Helsinki, 00790 Helsinki, Finland*

§*Global and Planetary Health, College of Public Health*

‖*Department of Molecular Medicine, Morsani College of Medicine*

⊥*University of South Florida, Tampa, Florida, 33612, United States of America*

#*Fachbereich Physik, Freie Universität Berlin, 14195 Berlin, Germany*

@*Department of Chemistry, University of Bergen, 5007 Bergen, Norway*

△*Computational Biology Unit, Department of Informatics, University of Bergen, 5008 Bergen, Norway*

∇*BioTechMed-Graz, 8010 Graz, Austria*

††*Field of Excellence BioHealthâĂŤUniversity of Graz, 8010 Graz, Austria*

E-mail: matti.javanainen@helsinki.fi; samuli.ollila@helsinki.fi

Abstract

Cholesterol is a central building block in biomembranes, where it induces orientational order, slows down diffusion, renders the membrane stiffer, and drives domain formation. Molecular dynamics (MD) simulations have played a crucial role in resolving these effects at the molecular level, yet it has recently become evident that different MD force fields predict quantitatively different behavior. Although easily neglected, identifying such limitations is increasingly important as the field rapidly progresses towards simulations of complex membranes mimicking the *in vivo* conditions: Pertinent multi-component simulations must capture accurately the interactions between their fundamental building blocks, such as phospholipids and cholesterol. Here, we define quantitative quality measures for simulations of binary lipid mixtures in membranes against C–H bond order parameters and lateral diffusion coefficients from NMR spectroscopy as well as form factors from X-ray scattering. Based on these measures, we perform a systematic evaluation on the ability of commonly used force fields to describe the structure and dynamics of binary mixtures of phosphatidylcholine and cholesterol. None of the tested force fields clearly outperforms the others across the tested properties and conditions, but the Slipids parameters provide the best overall performance. The quality-evaluation metrics introduced in this work will, particularly, foster future force field development and refinement for multi-component membranes using automated approaches.

1 Introduction

Cellular membranes contain an incredibly complex mixture of lipid molecules[1] unevenly distributed in the membrane plane and across its leaflets.[2–4] A key player driving the lateral heterogeneity is cholesterol (CHOL), which is present at concentrations from ∼10 mol-% (endoplasmic reticulum) up to ∼50 mol-% (plasma membrane, viral envelopes).[2] CHOL has the unique ability to order neighbouring lipids and thus induce the liquid-ordered (L_o) phase in model membranes.[5–8] In the cellular setting, the interaction between other lipids and

CHOL is associated with the formation of lipid rafts and nanodomains.[9,10] This heterogeneity can then further regulate protein distribution[11] or conformation,[12] in addition to the direct modulation of protein function.[13–15]

While the structure and dynamics of heterogeneous membranes are difficult to capture experimentally, atom-resolution molecular dynamics (MD) simulations have been employed to obtain a detailed view of the lateral organization driven by lipid–CHOL interactions.[8,16–19] Further MD efforts are facilitated by the growing availability of force fields with compatible lipid and protein parameters—enabling simulations of ever more complex and thus biologically relevant membranes.[1]

The traditional protein force fields CHARMM,[20] AMBER,[21] and OPLS[22,23] now have sizeable libraries of compatible lipid molecules, including CHOL, in the forms of CHARMM36,[24,25] Lipid17/Slipids,[26–31] and the force field by Maciejewski and Róg (here "MacRog"),[32–35] respectively. Notably, simulations using CHARMM36, Lipid17, and Slipids can these days be set up for multiple simulation engines with the CHARMM-GUI online tool; this decreases greatly the manual work needed to run complex membrane simulations.[36,37]

While simulating complex membranes with CHOL has become a relatively straightforward task, estimating the trustworthiness of MD simulations remains a challenge, especially as the complexity and number of membrane components increase. Our earlier work has demonstrated that the conformational ensembles of lipids from an MD simulation can be evaluated against the C–H bond order parameters from NMR experiments.[38–42] This approach has been useful for finding the best force fields to describe the headgroups of phosphatidylcholine (PC),[38,43] phosphatidylserine (PS),[41] phoshatidylethanolamine (PE)[42] and phosphatidylglycerol (PG) lipids,[42] to evaluate and improve membrane interactions with ions[40–42,44,45] and small molecules,[46] and to find simulation parameters predicting most realistic packing properties of membranes.[47,48] Furthermore, quantitative quality measures based on C–H bond order parameters have been recently defined and used to rank simulations in the NMRlipids Databank.[48] However, such automatic quality evaluation is limited to sim-

ulations for which experimental data at a corresponding composition and temperature are available. Because simulations mimicking all experimental compositions for multi-component membranes are often tedious to produce, quality evaluation of mixed lipid bilayers is not yet fully automatized in the NMRlipids Databank.

Here, we demonstrate how simulations of binary PC–CHOL mixtures can be evaluated against experimental NMR spectroscopy and X-ray scattering data by interpolating through multiple CHOL concentrations. As the effect of CHOL on lipid headgroup (and its independence from acyl chain ordering) has been discussed previously,[38,49] we focus here on the acyl chains; these are expected to play a larger role than the headgroup in CHOL-induced lateral membrane heterogeneity. We also evaluate the dependence of lateral diffusion coefficients on CHOL against pulsed field gradient (PFG) NMR experiments[50,51] using the recent theoretical framework that allows a quantitative comparison with experiment by eliminating finite-size effects in MD simulations.[52,53] With the structural and dynamic comparisons established, we then estimate the quality of four popular force fields at different CHOL concentrations. While we focus here on a PC–CHOL mixture, we expect our results to set guidelines for future efforts to validate intermolecular interactions in any binary or multi-component system.

2 Methods

2.1 X-ray Scattering Experiments

Fully hydrated multilamellar vesicles (MLVs), composed of POPC and CHOL with the latter present at 0–50 mol-% with 5 mol-% increments, were prepared for small angle X-ray scattering (SAXS) experiments using rapid solvent exchange as described previously.[54,55] This avoids the precipitation of CHOL crystallites at high concentration,[56] yielding non-phase separated samples up to 50 mol-% CHOL content. Lipids, purchased from Avanti Polar Lipids (Alabaster, AL, USA), were used as dry powders without any further purification. All other chemicals were obtained in pro analysis quality from Lactan (Graz, Austria). The

data were obtained at the EMBL BioSAXS beamline (Hamburg) using 20 keV photons at $T = 300$ K and analyzed in terms of the SDP-GAP model described in Refs. 57 and 58. The data from MLVs contain the structure factor (the crystalline lattice) and form factor in a convoluted fashion, yet by fitting the scattered intensity data we obtained both contributions. The electron density profiles were modelled from form factors using the SDP model, where volume distribution functions are described by individual Gaussians or error functions.[59–61] CHOL was described using two Gaussians, as detailed in Refs. 55 and 62. The membrane thickness was defined as twice the distance from the electron density maximum to the membrane center. The electron density maxima were extracted by the `findpeaks` function in Matlab.

2.2 Molecular Dynamics Simulations

We performed MD simulations of a pure POPC membrane as well as five POPC/CHOL mixtures with CHOL content ranging from 11 to 47 mol-%. Systems were simulated using four commonly used force fields: CHARMM36 (often abbreviated "C36" in figure legends in this work),[24,25] Amber-compatible Slipids[28–30] with its 2020 update,[31] Amber-compatible Lipid17,[26,27] and all-atom OPLS compatible MacRog.[33–35] To eliminate the finite size effects due to periodic boundary conditions from lateral diffusion coefficients of lipids, we performed all simulations in three sizes (64, 256, or 1024 POPC molecules). The number of POPC molecules was kept constant across the different CHOL concentrations. All membranes were solvated by 50 waters per lipid (POPC or CHOL). The small membranes (with 64 lipids) were first generated using CHARMM-GUI and equilibrated using the standard protocols for CHARMM36, Slipids, and Lipid17, for which inputs are readily available from CHARMM-GUI.[36,37] Then, the atomic coordinates were replicated in the membrane plane to create the 4- and 16-fold larger simulation systems. Since CHARMM-GUI does not support MacRog, the production simulations were initiated from equilibrated CHARMM36 structures, since the two force fields share the atom ordering. All simula-

tions were 1 s long, totaling 72 s, and performed using GROMACS version 2020 or 2021.[63] The first 10 ns of each simulation were omitted from analyses. The simulation parameters are provided in Table S1, and the simulation data are available at DOI: 10.5281/zenodo.7035350 (CHARMM36), DOI: 10.5281/zenodo.7022749 (Slipids), DOI: 10.5281/zenodo.6992065 (Lipid17), and DOI: 10.5281/zenodo.7061800 (MacRog). All simulations were added to the NMRlipids Databank[48] with the ID numbers listed in Table S2. The CHARMM36 simulations have been previously analyzed for their dynamic properties in Ref. 64.

Table 1: Details of the (small/medium/large) simulation systems. The box dimensions in the membrane plane (x and y) and normal to the membrane (z) are provided for the Slipids simulations, and the values vary slightly between the force fields.

[CHOL]	POPC	CHOL	Water	x and y (nm)	z (nm)
0 mol-%	64/256/1024	0/0/0	3200/12800/51200	4.4/9.0/18.1	8.9/8.6/8.5
11 mol-%	64/256/1024	8/32/128	3600/14400/57600	4.5/9.4/18.1	9.4/9.1/9.3
20 mol-%	64/256/1024	16/64/256	4000/16000/64000	4.5/9.2/18.3	10.2/9.9/10.0
29 mol-%	64/256/1024	26/104/416	4500/18000/72000	4.6/9.2/18.5	10.8/10.8/10.7
38 mol-%	64/256/1024	40/160/640	5200/20800/83200	4.8/9.5/19.2	11.3/11.4/11.2
47 mol-%	64/256/1024	56/224/896	6000/24000/96000	5.0/10.1/20.0	11.8/11.6/11.7

2.3 Simulation Analyses

Structural properties: The C–H bond order parameters, form factors, and electron density profiles, automatically calculated by the NMRlipids Databank,[48] were used. Similarly to the experimental X-ray scattering data, membrane thickness was defined as twice the distance from the electron density maximum to the membrane center. Locations of maxima were extracted by the `findpeaks` function in Matlab after smoothening the electron density data with the `smooth` function (5-point moving interval) in Matlab. Area per phospholipid was obtained by dividing the area of the bilayer (area of the simulation box) by the number of phospholipids in one leaflet.

To simplify the interpolation of order parameter data to intermediate CHOL concentra-

tions (see *"Quantitative quality evaluation of the effect of CHOL on membrane properties"* below), C–H bond order parameters of the 2 (3) hydrogens in CH_2 (CH_3) groups in the POPC acyl chains were averaged. These groups rotate freely and thus the order parameters are essentially identical for both (all) hydrogens in experiments and simulations. An exception to this are the hydrogens bound to the 2^{nd} carbon in the oleate chain; they lack rotational averaging in both simulations and experiments, and were thus treated separately in our analyses. The C–H order parameters for the POPC head group are shown separately for all CH_2 groups, *i.e.*, no averaging was performed.

Lateral Diffusion Coefficients: Lateral diffusion coefficients D_{PBC} from simulations performed using periodic boundary conditions (PBC) were extracted from mean squared displacement (MSD) data calculated for lipid centers of mass after eliminating the drift of their host leaflet with the `gmx msd` tool. The MSD data were fit with a straight line in the lag time (Δ) interval between 10 and 100 ns as

$$\text{MSD} = 4D_{\text{PBC}}\Delta. \tag{1}$$

The diffusion coefficients extracted from the three simulation box sizes (and thus membrane edge lengths L) were fitted with

$$D_{\text{PBC}} \approx D_\infty + \frac{k_{\text{B}}T}{4\pi\mu_{\text{m}}h}\frac{\ln\left[L/\left(L_{\text{SD}}+1.565H\right)\right]-1.713}{1+H/L_{\text{SD}}}, \tag{2}$$

where D_∞ is the lateral diffusion coefficient in an infinite system, h is the hydrodynamic thickness of the membrane, k_{B} is the Boltzmann constant, T is the temperature, H is half the thickness of the water layer, $L_{\text{SD}} = \frac{h\mu_{\text{m}}}{2\mu_{\text{f}}}$ the Saffman–Delbrück length, and μ_{m} and μ_{f} are shear viscosities of the membrane and the fluid (water), respectively.[53] Thus, the fit of Eq. (2) to the D_{PBC} values calculated from the simulation as a function of simulation box size L has two free parameters, namely D_∞ and μ_{m}, both of which are free of finite size

effects and can thus be compared to experiment. The inter-leaflet friction coefficient does not appear in Eq. (2) as we expect it to be infinite, which was found to be a valid assumption for lipid bilayers.[53] The water viscosity value of $\mu_f = 0.3228$ mPa·s was interpolated to 298 K from the values for CHARMM TIP3P in Ref. 65 and used for all simulations (CHARMM TIP3P and normal TIP3P differ by ∼2–3%). The simulation box dimensions (membrane edge length L and the dimension normal to the membrane plane (z) L_z) were taken from the final configuration of each simulation. L_z was only needed in the calculation of H (see below). Membrane thickness h was obtained as described in *"Structural properties"* above. As h and $H = (L_z - h)/2$ are constants in Eq. (2), the average values from the three systems sizes were used in the fits.

Quantitative quality evaluation of the effect of CHOL on membrane properties: To ease the evaluation of simulations against experimental data with non-matching CHOL concentrations, we interpolated the effect of CHOL in simulations and experiments for CHOL concentrations ranging from 0% to 46%. 2D matrices were created by interpolation for the oleate and palmitate chain order parameters (as a function of carbon atoms in the acyl chains and CHOL concentration) using the `interp2` function in Matlab based on linear interpolation. Similar matrices were also generated for the electron density profiles (as a function of normal distance from bilayer center and CHOL concentration) but with the `scatteredInterpolant` function in Matlab based on Delaunay triangulation.[66] Linear 1D interpolation with the `interp1` function in Matlab was used for the CHOL-dependence of the 1st and 2nd form factor minima locations and diffusion coefficients. These interpolations were then used to calculate deviations (in %) from experimental values across CHOL concentrations to quantify the quality of the lipid force fields. For the 2D matrices, the absolute values of the differences between matrices from simulations and experiments were first calculated. The averages of differences over the carbon atoms in the acyl chain (order parameters) or across the entire z coordinate in the simulation (density profiles) were then

calculated. This resulted in 1D deviation vectors as a function of CHOL concentration. For diffusion coefficients and form factor minima, the absolute value of the difference of the interpolated 1D vectors of simulation and experimental data was calculated to provide deviation as a function of CHOL concentration. All these 1D vectors were normalized by dividing them by the experimental values to provide relative deviations in % between a simulation and experiments as a function of CHOL concentration. For C–H bond order parameters, the deviation matrices between simulations and experiments were also used to illustrate quality of simulations.

3 Results and Discussion

3.1 Acyl Chain Ordering Varies Greatly Between the Force Fields

CHOL is known to induce order in lipid membranes by increasing the fraction of *anti* conformations in the acyl chains of phospholipids,[67] which is suggested to play a critical role in the phase behaviour of PC–CHOL mixtures.[6] Consequently, the correct CHOL-induced ordering is expected to be a necessary condition for a force field used to understand lipid–CHOL phase behaviour. The CHOL-induced ordering can be experimentally quantified by measuring the C–H bond order parameters using ^{13}C or ^{2}H NMR, and the results can also be directly compared to MD simulations.[39] Simulations generally show some CHOL-induced ordering, but the order parameter values often deviate from the experimental ones at high CHOL concentrations.[27,67] Furthermore, it has not been clear how accurately different force fields capture the details of lipid–CHOL interactions, and which force field would give most realistic results for simulations of complex mixtures, where such interactions play critical roles.

Here, we evaluate the CHOL-induced ordering in state-of-the-art force fields against C–H bond order parameter data from ^{13}C NMR experiments measured from POPC–CHOL mixtures with CHOL concentrations ranging between 0 and 60 mol-%.[67] To this end, we first

interpolated order parameter maps as a function of acyl chain carbon number and CHOL concentration for both simulations and experiments. These maps were then subtracted to obtain deviation maps between simulations and experiments. The deviation maps of different force fields are shown for the palmitate (top row) and oleate (bottom row) chains of POPC in Fig. 1, whereas the original order parameter profiles are shown in Figs. S6 and S7 for the palmitate and oleate chains, respectively.

In all simulation force fields and experiments, the CHOL-induced ordering is manifested in the original profiles (Figs. S6 and S7) as a substantial increase in the absolute values of acyl chain C–H bond order parameters upon addition of CHOL. The deviations mapped in Fig. 1 provide an intuitive view for a quantitative comparison of different force fields against experiments: In white regions, the simulation results are considered to fall within the experimental error as the deviations are in the range of [–0.02,0.02]; blue indicates that the order parameters are too negative, *i.e.*, the acyl chains are too ordered in simulations, and *vice versa* for red. Overall, the simulation force fields behave reasonably well at low CHOL concentrations, but deviate significantly from experiment at higher CHOL concentrations.

In CHARMM36, both the palmitate and oleate chains get too ordered upon increasing CHOL concentration. The oleate chain shows best agreement with experiment in Slipids, whereas there is some excess ordering in the palmitate chain. Still, the major discrepancy between Slipids and experiment is the drastically too disordered C2 and C3 carbons of the palmitate chain. This effect was introduced in the recent reparametrization of Slipids that improved the head group and glycerol backbone structures of Slipids.[31] Lipid17 provides the best overall agreement with experiment, as no segments deviate significantly from experiment at any CHOL concentrations. MacRog behaves reasonably well at low CHOL concentrations, yet at larger CHOL concentrations the chains become too ordered, leading to the largest overall deviations from experiment. For the head group and glycerol backbone order parameters, provided in Fig. S8, CHARMM36 gives the best agreement at all cholesterol concentrations, in line with previous studies.[38,49]

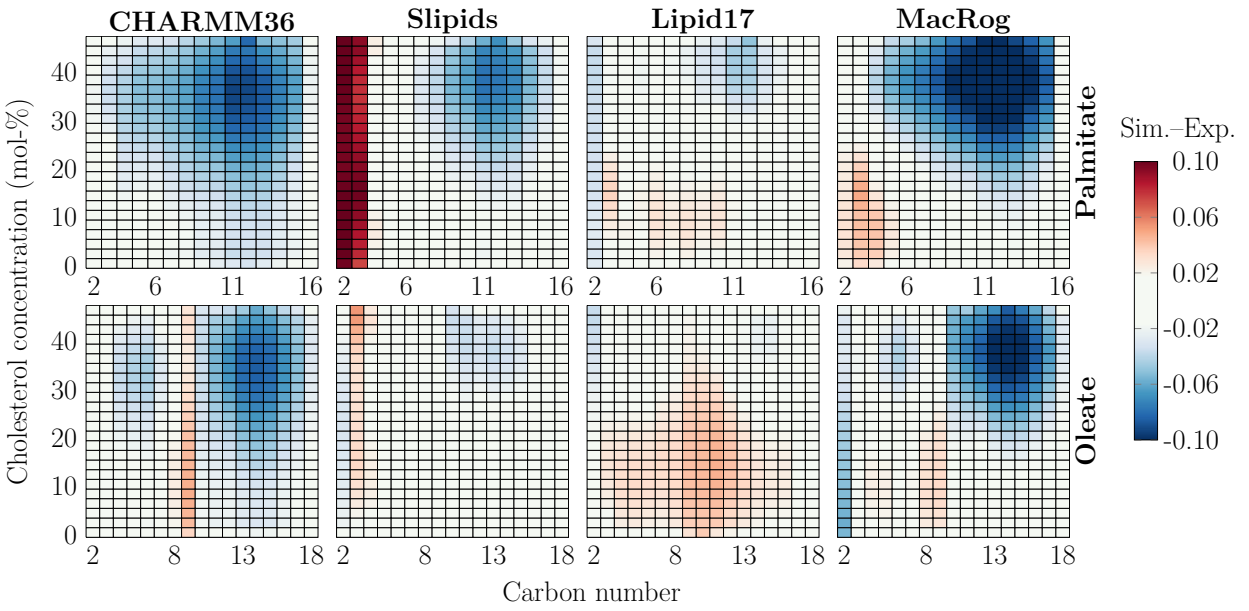

Figure 1: POPC acyl chain order parameter deviation from experiments. Data are shown for palmitate (top row) and oleate (bottom row) and for the four force fields (columns). Negative values indicate that order is too high (S_{CH} values too negative) in the simulations. The values that are within the estimated experimental error range of ± 0.02[39] are coloured white. Statistical error in simulations is not considered here because it is approximately order of magnitude smaller than the experimental error. Order parameters of hydrogens attached to the same carbon were averaged, except for the C2 carbon of the oleate chain (whose order parameters forked) for which differences for both the larger and smaller values were calculated, and the average of these differences is shown in the C2 column.

3.2 Cholesterol Effect on Membrane Properties is Manifested Differently in Different Force Fields

CHOL-induced ordering straightens the acyl chain conformations, which leads to membrane thickening. While acyl chain order and membrane thickness are well correlated,[48] lipid bilayer dimensions can be accessed more directly by measuring the X-ray form factor, which is related to the electron density along membrane normal *via* Fourier transform.[39,58,68,69] Electron density profile, area per phospholipid, and bilayer thickness can all be extracted from the form factor using the scattering density profile (SDP) model or its combination with MD simulations.[58,60,68–70] To complement the evaluation of CHOL-induced ordering against NMR order parameters, we measured also the X-ray form factors from POPC–CHOL mixtures at

systematically increasing CHOL concentrations. Scattering intensities from experiments are shown in Figs. S1 and S2, form factors from experiments and simulations in Fig. S3, and density profiles in Fig. S4.

The effect of CHOL on structural properties of bilayers is compared between the SDP model (based on experimental form factors) and MD simulation results in Fig. 2. All force fields demonstrate increasing thickness upon addition of CHOL that tends to saturate after approximately 30 mol-% (bottom middle panel in Fig. 2). Most MD simulations agree well with the SDP model below 30 mol-%, but overshoot the SDP results at high CHOL concentrations. Lipid17 simulations are the exception: They predict thinner membranes than the SDP model at low CHOL concentrations, and a clear saturation of thickness increase is not observed, unlike for other force fields and experiments.

The dependence of the area per phospholipid (APL) on CHOL concentration follows the trends in thickness inversely in general (bottom right panel of Fig. 2), yet provides curious differences between force fields at the physiologically relevant CHOL concentration range.[2] Lipid17 has the largest APL across the entire CHOL contration range. MacRog also has a large APL for pure POPC, but the partial area of CHOL is negative until 30 mol-% concentration, indicating a particularly strong condensation effect. The profiles for Slipids and CHARMM36 are very similar, with a small or zero partial area of CHOL until a concentration of 20 mol-%.

For more detailed comparison of membrane structure, we interpolated the changes in electron density profiles along membrane normal (Fig. S4) as a function of CHOL concentration to create two-dimensional electron density maps (Fig. 2). Overall, all electron density profiles share the same features across all CHOL concentrations: High-densities band corresponding to the tightly-packed interfacial regions containing the electron-rich phosphorus, low density at the core of the membrane occupied by the disordered acyl chains, and intermediate density in the rest of the lipid regions as well as the aqueous phase. However, a more detailed look at the profiles in Fig. 2 reveals differences between the force fields and the

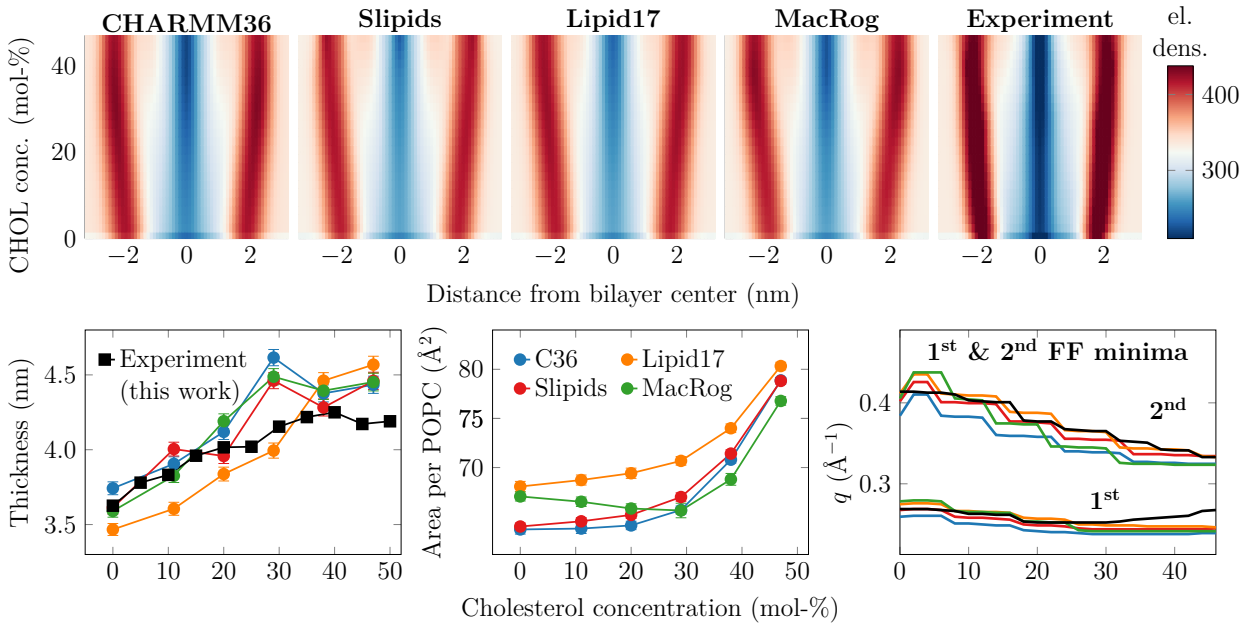

Figure 2: **Electron density profiles, thickness, and area per phospholipid as a function of CHOL concentration.** Top: Electron density maps for the simulations using four different force fields and for the experiment (from the SDP model). The colorbar is common for all maps. The original electron density profiles are shown in Fig. S4. The effect of system size on the density profiles in simulations is demonstrated in Fig. S12 in the SI. Bottom left: Bilayer thickness. Thickness is defined as twice the distance from the peak in electron density to the membrane core. Experimental data are extracted in a similar manner from electron density profiles obtained with X-ray scattering. The bin width used in the profiles is used as the error estimate. Bottom middle: area per phospholipid measured by dividing the total membrane area by the number of phospholipids. The size-dependency of the area per phospholipid is shown in Fig. S11. Bottom right: Effect of CHOL on the location of the first two minima in the form factor. The minima are extracted from the form factors interpolated to all CHOL concentrations (Fig. S3) from experiment and simulation with the `findpeaks` function in Matlab.

SPD model. CHARMM36 has the sharpest low- and high-density bands among MD simulation results, indicating smaller membrane undulations that would smear the bands; the same is true for MacRog at higher CHOL concentrations. The less sharp bands for Lipid17 and especially Slipids profiles indicate that their membranes are more flexible. The SDP model gives the sharpest bands (bottom left panel in Fig. 2 and original electron density profiles in Fig. S4), suggesting more uniform membrane structure than any MD simulation. However, system size plays a role here as undulations smear out the density profile features

with increasing simulation box size as demonstrated in Fig. S12 by the density maps calculated for the CHARMM36 simulations in three sizes. Still, even in the smallest system, the band intensities are less localized than in the SDP model. This might indicate different elastic properties between simulation and experiment, but we cannot fully exclude the role of models used to interpret scattering data.

Nevertheless, the minima in X-ray form factors are independent of the simulation box size and correlate with membrane dimensions.[48] For a more direct comparison between simulations and experiments, we thus interpolated the locations of first two minima in the form factors over the entire studied range of CHOL concentrations (bottom right panel of Fig. 2). Because differences between experiments and simulations for the 1st minimum location are barely visible for some force fields, we have highlighted the relative deviations in Fig. S5. These curves highlight that at first the addition of CHOL shifts the first minima to smaller wave vector values in the experiment; this is reasonably well captured by the simulation force fields, although CHARMM36 seems to be off more than the other three force fields. Above ∼25 mol-% of CHOL, the location of the minimum shifts to larger wave vector values in the experiment, which is curiously not captured by any of the force fields. For the second minimum, the experiment shows a steady shift to smaller wave vector values; this is reproduced by all simulation force fields, but Slipids and Lipid17 are generally in better agreement with the experiment than MacRog and CHARMM36.

3.3 The Force Fields Predict Very Different Lateral Mobilities

Apart from the ordering effect on the bilayer structure, CHOL is also known to make bilayers stiffer and less dynamic.[8,50,51] The comparison between lateral diffusion coefficients extracted from simulation and experiment has been limited due to a box-size dependence observed in simulations performed using periodic boundary conditions.[52,53,71] Here, we tackle this issue by performing simulations with three system sizes, which allows the extrapolation of the results to an infinite system with the theoretical description developed by VÃűgele and Hummer.[52,53]

The size-dependence of phospholipid lateral diffusion from simulations together with the fit of Eq. (2) are shown in Fig. S9, whereas the CHOL-dependence of these values in systems with different sizes are shown in Fig. S10. The PBC-corrected lateral diffusion coefficients of POPC are shown in the top panel of Fig. 3 together with experimental values from ^{1}H pulsed field gradient NMR diffusion measurements on label-free macroscopically aligned bilayers.[50,51]

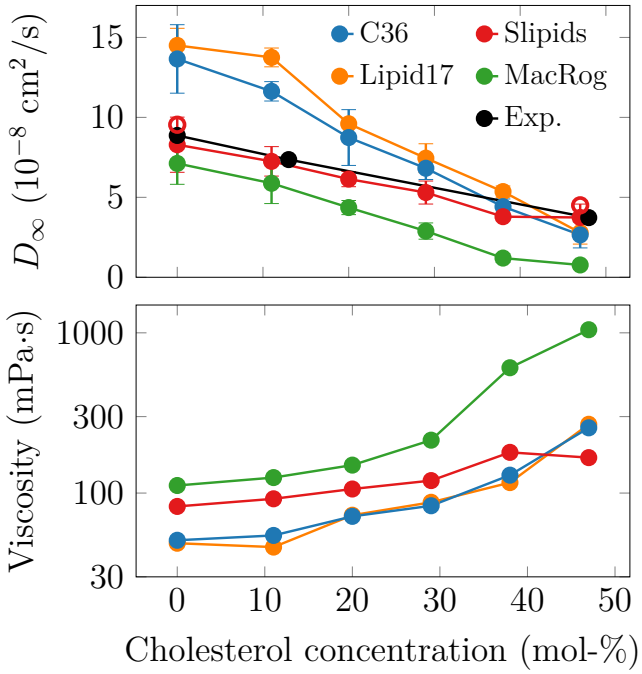

Figure 3: **Dynamic properties of the POPC/CHOL mixtures.** Top: POPC lateral diffusion coefficients corrected for finite-size effects using Eq. (2). Experimental data are taken from NMR measurements of well-hydrated samples.[50,51] The hollow circles show data extracted for Slipids using a shorter Lennard-Jones cutoff (see text). The error bars show the standard deviations of the diffusion coefficients obtained from 10,000 fits to the values $D \pm \Delta D$, where ΔD are sampled from normal distributions whose standard deviations are equal to the error estimates of the corresponding values of D. For these error estimates, we used the differences of the diffusion coefficients extracted from the two membrane leaflets. Bottom: Shear viscosities obtained from the finite-size correction, Eq. (2). The size-dependence of lateral diffusion and the fits used to obtain the PBC-corrected diffusion coefficients and shear viscosities are shown in Figs. S9 and S10.

The lipid force fields again show significantly different behavior. Lipid17 and CHARMM36 show too fast dynamics for pure POPC, and the slow-down induced by CHOL is exaggerated as compared to experiment. Diffusion in MacRog is generally too slow, yet Slipids provides

an essentially quantitative agreement with experiment across the studied CHOL concentrations, and thus significantly outperforms the other force fields in terms of lateral dynamics. Interestingly, there is no correlation in the deviations from experiments between the lateral dynamics and the structural properties described earlier. To investigate if the differences in lateral diffusion coefficients could be explained by different Lennard-Jones (LJ) cutoff values, we repeated simulations at 0 mol-% and 47 mol-% CHOL for Slipids using a shorter cutoff of 0.9 nm (corresponding to that of Lipid17, while original cutoff for Slipids was 1.4 nm, see Table S1). The PBC-corrected diffusion coefficient values with shorter cutoff, shown in the top panel of Fig. 3 as hollow red circles, are only slightly larger than the original values, indicating that differences arise from a combination of force field interaction parameters, and are not explained by the LJ cutoff alone.

When comparing lipid lateral diffusion between simulations and experiments, it is important to note that the PBC correction does not only affect values of diffusion coefficients but also qualitatively changes their trends as a function of cholesterol. This results from the fact that the size of the PBC correction, Eq. (2), depends on membrane viscosity, which further depends on CHOL concentration. For example, Fig. S10 would indicate that Lipid17 and CHARMM36 systemically underestimate the experimental values in systems with all sizes simulated here, while the effect of CHOL seems to be qualitatively reproduced. However, their PBC-corrected values significantly overshoot the experiment at low CHOL concentration, and CHOL induces a more drastic slowdown in simulations, leading to values close to experimental ones at 47 mol-% CHOL. With MacRog, also the PBC-corrected values fall below the experimental ones, yet the slowdown effect of CHOL still appears stronger than in experiment. With Slipids, the CHOL-dependence seems too weak with finite system sizes, yet after accounting for PBC effects, the agreement with experiment is excellent. These results underline that little can be said about the CHOL-dependence of lateral diffusion coefficients without the PBC correction that requires performing simulations with multiple box sizes at different CHOL concentrations. Consequently, fine-tuning of interaction pa-

rameters to correctly reproduce lateral diffusion coefficients can require massive number of simulations.

We also provide the shear viscosity values of the membranes obtained from the fits of Eq. (2) in Fig. 3. Direct comparison of these to experimental values is complicated due to the large scatter of experimental estimates,[72] yet values from Slipids are expected to be most realistic because its lateral diffusion coefficients are closest to experiments. Note that the viscosities from CHARMM36 simulations are further discussed in our previous work.[64]

3.4 Quality of Force Fields at Various Cholesterol Concentrations

To streamline the selection of force fields that best capture the effect of CHOL on different membrane properties, we defined quantitative quality measures for simulations. For this we calculated for all the force fields their relative deviations from experiments (difference between simulated and experimental values divided by the experimental value) using interpolated data for the form factor minima, the order parameters of the two acyl chains, and the diffusion coefficients. The quality evaluations are shown in Fig. 4.

The quality evaluations reveal that Slipids provides the overall best agreement with experiment, yet its quality decreases slightly at higher CHOL concentrations. Lipid17 provides a slightly better agreement with experiment above ∼30 mol-% of CHOL than Slipids, but exhibits major deviation from experiments at low CHOL concentrations. MacRog performs relatively well at low CHOL concentrations, but its quality deteriorates significantly upon the addition of CHOL. The deviation for CHARMM36 is significant at all CHOL concentrations.

4 Conclusions

The tested all-atom force fields captured the most important general effects of CHOL on membrane properties: increased acyl chain ordering, concomitant increase in bilayer thickness, and reduced lateral diffusion rate of phospholipids. However, quantitative comparison

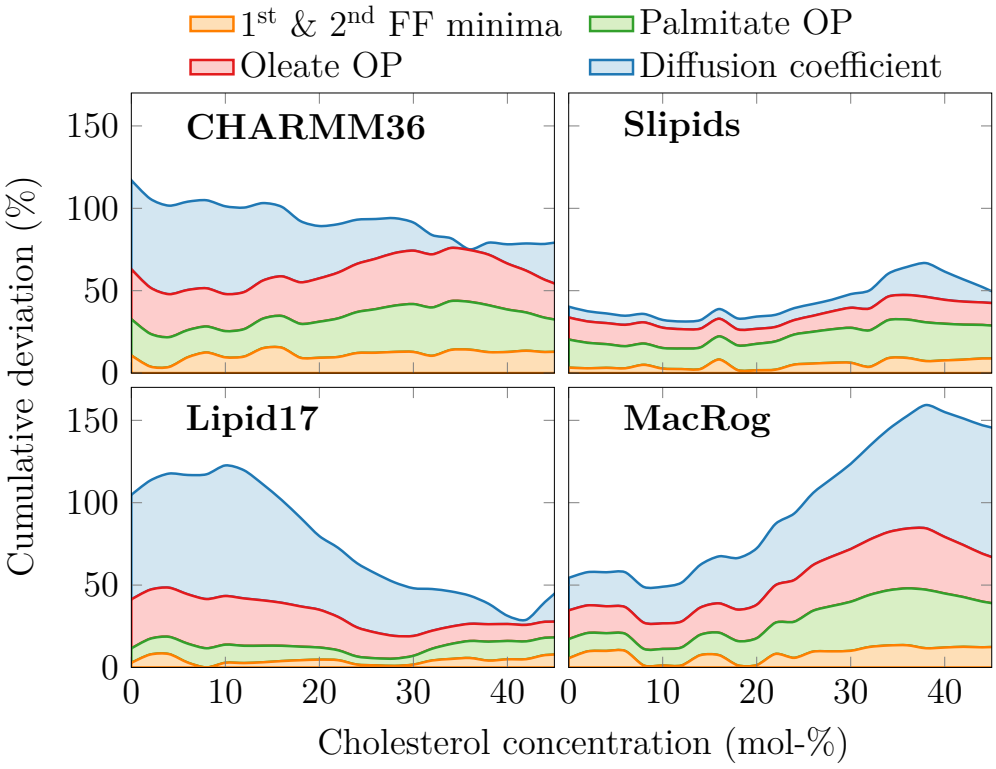

Figure 4: **Total relative deviation of force fields from experimental data.** Two leftmost columns: The relative deviations in the first two form factor minima, palmitate and oleate chain order parameters, and diffusion coefficients shown in a cumulative manner to highlight the overall deviation of the force fields from experimental data. The order parameter deviations are obtained by averaging over the columns in Fig. 1 and normalizing against experimental data. For the form factor minima (shown in the bottom right panel) the deviation was obtained by calculating the difference between experiment and simulation for both minima, normalizing each against experimental data, and summing the two together. The diffusion coefficient deviation is the difference of values from simulation and experiment in Fig. 3, taken after interpolation to the same CHOL values as shown in Figs. 1 and 2, and normalized against experimental values. Top right panel: The zoomed-in view to the deviation in the location of the first minimum in the form factor.

reveals differences between force fields and their qualities evaluated against NMR and X-ray scattering data. Comparison with NMR order parameters and X-ray scattering form factors propose that simulations reproduce experimental results until up to 20 mol-% of CHOL, but overestimate the acyl chain ordering and membrane thickness after further addition of CHOL. An apparent exception to this is the Lipid17 force field, yet its seemingly better agreement with experiments results from compensation of intially (at low CHOL concentra-

tions) underestimated acyl chain order by the overly strong response to the CHOL addition. In conclusion, a unified picture emerging from comparison with NMR and X-ray scattering data suggests that all the tested force fields overestimate the CHOL ordering effect, particularly above 20 mol-% of CHOL. A previously published comparison[67] suggested the same conclusion for the historically relevant Berger/Höltje force field parameters[73,74] that were not included in this work.

Besides the CHOL-induced ordering, effects on membrane properties have been discussed also in terms of (i) the CHOL condensing effect, which refers to a decrease in the *area per phospholipid* upon the addition of CHOL (negative partial area),[75] or (ii) CHOL having a diminishing partial area, meaning that a certain amount of CHOL could be added to a phospholipid bilayer without effecting its total area (zero partial area).[76] At the physiological CHOL concentrations in the range from 0 to 30 mol-%, only MacRog predicts negative partial area for CHOL, while CHARMM36 predicts zero partial area, and Slipids and Lipid17 predict small positive partial areas. Considering that Slipids and Lipid17 perform best in our quality evaluation against experiments, yet still slightly overestimating the CHOL condensing effect, our results suggest that CHOL has a positive but small partial area.

Considering also lateral dynamics and previous evaluation of rotational dynamics against NMR data,[77] Slipids is overall closest to experiments among the parameters tested here, and is therefore probably the best choice for studies where lipid–CHOL interactions play major role. Nevertheless, all tested parameters capture qualitative effects of CHOL on membrane properties relatively well and differences between force fields are clearly smaller than, for example, in the case of PC–PS lipid mixtures.[47] Therefore, the quality of the force field selected for other molecules, such as lipids other than phosphatidylcholine, proteins, sugars, or drugs together with force field compatibility might be a more relevant decisive factor for simulations of complex systems. Finally, it must be noted that while all simulations were performed with their suggested simulation parameters, the different simulation engines might provide slightly different behavior, yet we believe that evaluating the magnitude of

such effects is well beyond the scope of this work.

Our results demonstrate that quality evaluation of lipid mixture simulations against experimental NMR and X-ray scattering data give consistent results for how accurately force field parameters capture intermolecular interactions. The interpolation approach introduced here extends the NMRlipids Databank quality metrics[48] beyond individual systems: this enables automatic ranking of not only lipid mixtures but also of membranes mixed with other molecules such as ions. Such tools will strongly support the emerging endeavours for automatic improvement of force field parameters.[47]

Supporting Information Available

Simulation parameters used for all the studied force fields. Form factor plots from simulations and experiments with the traced minima at various cholesterol concentrations. Electron density profiles from simulation and experiment at various cholesterol concentrations. Deuterium order parameters of both acyl chains of POPC from simulation and experiment at various cholesterol concentrations. Deviation of POPC head group order parameters from experiment as a function of cholesterol concentration. Lateral diffusion coefficients with varying cholesterol concentrations as a function of simulation box size from simulations together with the extrapolation of these values to an infinite box size. Diffusion coefficients as a function of cholesterol concentration from simulations with varying box sizes together with comparison to experiment. Effect of simulation box size on the area per phospholipid across the studied cholesterol concentrations. Effect of simulation box size on the density profiles across the studied cholesterol concentrations. Cholesterol tilt as a function of cholesterol concentration from simulations. This material is available free of charge via the Internet at `http://pubs.acs.org/`.

Acknowledgement

We acknowledge CSC – IT Center for Science for computational resources. MJ (grant no. 338160) and OHSO (grant nos. 315596 & 319902) thank the Academy of Finland for funding.

Author contributions statement

MJ performed all simulations. MJ and OHSO conceptualized the manuscript, analyzed all simulations and wrote the manuscript. PH performed and analyzed all SAXS experiments. GP designed SAXS experiments and revised the manuscript. JJM contributed to early testing (debugging, setup, and running) of simulations with the Amber force field and manuscript editing. MSM contributed to initial planning of the work and revised the manuscript.

References

(1) Lorent, J.; Levental, K.; Ganesan, L.; Rivera-Longsworth, G.; Sezgin, E.; Doktorova, M.; Lyman, E.; Levental, I. *Nat. Chem. Biol.* **2020**, *16*, 644–652.

(2) Van Meer, G.; Voelker, D. R.; Feigenson, G. W. *Nat. Rev. Mol. Cell. Biol.* **2008**, *9*, 112–124.

(3) Wang, H.-Y.; Bharti, D.; Levental, I. *Front. Cell Dev. Biol.* **2020**, *8*, 580814.

(4) Kinnun, J. J.; Bolmatov, D.; Lavrentovich, M. O.; Katsaras, J. *Chem. Phys. Lipids* **2020**, *232*, 104976.

(5) Mouritsen, O. G.; Zuckermann, M. J. *Lipids* **2004**, *39*, 1101–1113.

(6) Ipsen, J. H.; Karlström, G.; Mouritsen, O.; Wennerström, H.; Zuckermann, M. *Biochim. Biophys. Acta* **1987**, *905*, 162–172.

(7) Kinnunen, P. K. *Chem. Phys. Lipids* **1991**, *57*, 375–399.

(8) Róg, T.; Pasenkiewicz-Gierula, M.; Vattulainen, I.; Karttunen, M. *Biochim. Biophys. Acta* **2009**, *1788*, 97–121.

(9) Simons, K.; Ikonen, E. *Nature* **1997**, *387*, 569–572.

(10) Cebecauer, M.; Amaro, M.; Jurkiewicz, P.; Sarmento, M. J.; Sachl, R.; Cwiklik, L.; Hof, M. *Chem. Rev.* **2018**, *118*, 11259–11297.

(11) Milovanovic, D.; Honigmann, A.; Koike, S.; Göttfert, F.; Pähler, G.; Junius, M.; Müllar, S.; Diederichsen, U.; Janshoff, A.; Grubmüller, H.; Eggeling, C.; Hell, S. W.; van den Bogaart, G.; Jahn, R. *Nat. Commun.* **2015**, *6*, 1–10.

(12) Kelkar, D. A.; Chattopadhyay, A. *Biochim. Biophys. Acta* **2007**, *1768*, 1103–1113.

(13) Gimpl, G. *Chem. Phys. Lipids* **2016**, *199*, 61–73.

(14) Guixà-González, R.; Albasanz, J. L.; Rodriguez-Espigares, I.; Pastor, M.; Sanz, F.; Martí-Solano, M.; Manna, M.; Martinez-Seara, H.; Hildebrand, P. W.; Martín, M.; Selent, J. *Nat. Commun.* **2017**, *8*, 1–12.

(15) Manna, M.; Niemelä, M.; Tynkkynen, J.; Javanainen, M.; Kulig, W.; Müller, D. J.; Rog, T.; Vattulainen, I. *eLife* **2016**, *5*, e18432.

(16) Róg, T.; Vattulainen, I. *Chem. Phys. Lipids* **2014**, *184*, 82–104.

(17) Berkowitz, M. L. *Biochim. Biophys. Acta* **2009**, *1788*, 86–96.

(18) Enkavi, G.; Javanainen, M.; Kulig, W.; Róg, T.; Vattulainen, I. *Chem. Rev.* **2019**, *119*, 5607–5774.

(19) Marrink, S. J.; Corradi, V.; Souza, P. C.; Ingolfsson, H. I.; Tieleman, D. P.; Sansom, M. S. *Chem Rev.* **2019**, *119*, 6184–6226.

(20) Brooks, B. R.; Bruccoleri, R. E.; Olafson, B. D.; States, D. J.; Swaminathan, S. a.; Karplus, M. *J. Comput. Chem.* **1983**, *4*, 187–217.

(21) Cornell, W. D.; Cieplak, P.; Bayly, C. I.; Gould, I. R.; Merz, K. M.; Ferguson, D. M.; Spellmeyer, D. C.; Fox, T.; Caldwell, J. W.; Kollman, P. A. *J. Am. Chem. Soc.* **1995**, *117*, 5179–5197.

(22) Jorgensen, W. L.; Tirado-Rives, J. *J. Am. Chem. Soc* **1988**, *110*, 1657–1666.

(23) others,, et al. *J. Chem. Theory Comput.* **2016**, *12*, 281–296.

(24) *Biophys. J.* **2006**, *90*, 2796–2807.

(25) Lim, J. B.; Rogaski, B.; Klauda, J. B. *J. Phys. Chem. B* **2012**, *116*, 203–210.

(26) Dickson, C. J.; Madej, B. D.; Skjevik, A. A.; Betz, R. M.; Teigen, K.; Gould, I. R.; Walker, R. C. *J. Chem. Theory Comput.* **2014**, *10*, 865–879.

(27) Madej, B. D.; Gould, I. R.; Walker, R. C. *J. Phys. Chem. B* **2015**, *119*, 12424–12435.

(28) Jämbeck, J. P. M.; Lyubartsev, A. P. *J. Phys. Chem. B* **2012**, *116*, 3164–3179.

(29) Jämbeck, J. P. M.; Lyubartsev, A. P. *J. Chem. Theory Comput.* **2012**, *8*, 2938–2948.

(30) JÃďmbeck, J. P. M.; Lyubartsev, A. P. *J. Chem. Theory Comput.* **2013**, *9*, 774–784.

(31) Grote, F.; Lyubartsev, A. P. *J. Phys. Chem. B* **2020**, *124*, 8784–8793.

(32) Maciejewski, A.; Pasenkiewicz-Gierula, M.; Cramariuc, O.; Vattulainen, I.; Róg, T. *J. Phys. Chem. B* **2014**, *118*, 4571–4581.

(33) Kulig, W.; Tynkkynen, J.; Javanainen, M.; Manna, M.; Róg, T.; Vattulainen, I.; Jungwirth, P. *J. Mol. Model.* **2014**, *20*.

(34) Kulig, W.; Jurkiewicz, P.; Olżyńska, A.; Tynkkynen, J.; Javanainen, M.; Manna, M.; Róg, T.; Hof, M.; Vattulainen, I.; Jungwirth, P. *Biochim. Biophys. Acta* **2015**, *1848*, 422–432.

(35) Kulig, W.; Pasenkiewicz-Gierula, M.; Róg, T. *Chem. Phys. Lipids* **2016**, *195*, 12–20.

(36) Lee, J.; Cheng, X.; Swails, J. M.; Yeom, M. S.; Eastman, P. K.; Lemkul, J. A.; Wei, S.; Buckner, J.; Jeong, J. C.; Qi, Y.; Jo, S.; Pande, V. S.; Case, D. A.; Brooks, C. L.; MacKerell, A. D.; Klauda, J. B.; Im, W. *J. Chem. Theory Comput.* **2016**, *12*, 405–413.

(37) Lee, J.; Hitzenberger, M.; Rieger, M.; Kern, N. R.; Zacharias, M.; Im, W. *J. Chem. Phys.* **2020**, *153*, 035103.

(38) Botan, A.; Favela-Rosales, F.; Fuchs, P. F. J.; Javanainen, M.; Kanduč, M.; Kulig, W.; Lamberg, A.; Loison, C.; Lyubartsev, A.; Miettinen, M. S.; Monticelli, L.; Määttä, J.; Ollila, O. H. S.; Retegan, M.; Róg, T.; Santuz, H.; Tynkkynen, J. *J. Phys. Chem. B* **2015**, *119*, 15075–15088.

(39) Ollila, O. S.; Pabst, G. *Biochim. Biophys. Acta* **2016**, *1858*, 2512–2528.

(40) others,, et al. *Phys. Chem. Chem. Phys.* **2016**, *18*, 32560–32569.

(41) others,, et al. *J. Phys. Chem. B* **2019**, *123*, 9066–9079.

(42) others,, et al. *J. Am. Chem. Soc.* **2021**, *143*, 13701–13709.

(43) Kurki, M.; Poso, A.; Bartos, P.; Miettinen, M. S. *J. Chem. Inf. Model.* **2022**, *62*, 6462–6474.

(44) Melcr, J.; Martinez-Seara, H.; Nencini, R.; Kolafa, J.; Jungwirth, P.; Ollila, O. H. S. *J. Phys. Chem. B* **2018**, *122*, 4546–4557.

(45) Melcr, J.; Mendes Ferreira, T.; Jungwirth, P.; Ollila, O. S. *J. Chem. Theory Comput.* **2019**, https://doi.org/10.1021/acs.jctc.9b00824.

(46) Nencini, R.; Ollila, O. H. S. *J. Phys. Chem. B* **2022**, *126*, 6955–6963.

(47) Antila, H. S.; Kav, B.; Miettinen, M. S.; Martinez-Seara, H.; Jungwirth, P.; Ollila, O. S. *J. Phys. Chem. B* **2022**, *126*, 4169–4183.

(48) Kiirikki, A. M.; Antila, H. S.; Bort, L.; Buslaev, P.; Favela, F.; Ferreira, T. M.; Fuchs, P. F.; Garcia-Fandino, R.; Gushchin, I.; Kav, B.; Kula, P.; Kurki, M.; Kuzmin, A.; Madsen, J. J.; Miettinen, M. S.; Nencini, R.; Piggot, T.; Pineiro, A.; Samantray, S.; Suarez-Leston, F.; Ollila, O. H. S. NMRlipids Databank: Making Data-Driven Analyses of Membrane Properties Accessible for All. 2023; `https://doi.org/10.26434/chemrxiv-2023-jrpwm`.

(49) Antila, H. S.; Wurl, A.; Ollila, O. S.; Miettinen, M. S.; Ferreira, T. M. *Biophys. J.* **2022**, *121*, 68–78.

(50) Filippov, A.; Orädd, G.; Lindblom, G. *Biophys. J.* **2003**, *84*, 3079–3086.

(51) Filippov, A.; Orädd, G.; Lindblom, G. *Langmuir* **2003**, *19*, 6397–6400.

(52) VÃűgele, M.; Hummer, G. *J. Phys. Chem. B* **2016**, *120*, 8722–8732.

(53) Vögele, M.; Köfinger, J.; Hummer, G. *Phys. Rev. Lett.* **2018**, *120*, 268104.

(54) Rieder, A.; Koller, D.; Lohner, K.; Pabst, G. *Chem. Phys. Lipids* **2015**, *186*, 39–44.

(55) Belička, M.; Weitzer, A.; Pabst, G. *Soft Matter* **2017**, *13*, 1823–1833.

(56) Buboltz, J. T.; Feigenson, G. W. *Biochim. Biophys. Acta* **1999**, *1417*, 232–245.

(57) Heftberger, P.; Kollmitzer, B.; Heberle, F. A.; Pan, J.; Rappolt, M.; Amenitsch, H.; Kučerka, N.; Katsaras, J.; Pabst, G. *J. Appl. Crystallogr.* **2014**, *47*, 173–180.

(58) Heftberger, P.; Kollmitzer, B.; Rieder, A. A.; Amenitsch, H.; Pabst, G. *Biophys. J.* **2015**, *108*, 854–862.

(59) Heberle, F.; Pan, J.; Standaert, R.; Drazba, P.; Kučerka, N.; Katsaras, J. *Eur. Biophys. J.* **2012**, *41*, 875–890.

(60) Kučerka, N.; Nagle, J. F.; Sachs, J. N.; Feller, S. E.; Pencer, J.; Jackson, A.; Katsaras, J. *Biophys. J.* **2008**, *95*, 2356–2367.

(61) Kučerka, N.; Holland, B. W.; Gray, C. G.; Tomberli, B.; Katsaras, J. *J. Phys. Chem. B* **2012**, *116*, 232–239.

(62) Heftberger, P. Structure and Elasticity of Fluid Membrane Domains. Ph.D. thesis, Graz University of Technology, 2015.

(63) Páll, S.; Zhmurov, A.; Bauer, P.; Abraham, M.; Lundborg, M.; Gray, A.; Hess, B.; Lindahl, E. *J. Chem. Phys.* **2020**, *153*, 134110.

(64) Fabian, B.; Vattulainen, I.; Javanainen, M. *Accepted to J. Chem. Theory Comput.* **2023**, 2023–02.

(65) Ong, E. E.; Liow, J.-L. *Fluid Ph. Equilibria* **2019**, *481*, 55–65.

(66) Amidror, I. *J. Electron. Imaging* **2002**, *11*, 157–176.

(67) Ferreira, T. M.; Coreta-Gomes, F.; Ollila, O. H. S.; Moreno, M. J.; Vaz, W. L. C.; Topgaard, D. *Phys. Chem. Chem. Phys.* **2013**, *15*, 1976–1989.

(68) Pan, J.; Cheng, X.; Heberle, F. A.; Mostofian, B.; Kučerka, N.; Drazba, P.; Katsaras, J. *J. Phys. Chem. B* **2012**, *116*, 14829–14838.

(69) Marquardt, D.; Heberle, F. A.; Nickels, J. D.; Pabst, G.; Katsaras, J. *Soft Matter* **2015**, *11*, 9055–9072.

(70) Doktorova, M.; KuÄDerka, N.; Kinnun, J. J.; Pan, J.; Marquardt, D.; Scott, H. L.; Venable, R. M.; Pastor, R. W.; Wassall, S. R.; Katsaras, J.; Heberle, F. A. *J. Phys. Chem. B* **2020**, *124*, 5186–5200.

(71) Camley, B. A.; Lerner, M. G.; Pastor, R. W.; Brown, F. L. *J. Chem. Phys.* **2015**, *143*, 12B604_1.

(72) Faizi, H. A.; Dimova, R.; Vlahovska, P. M. *Biophys. J.* **2022**, *121*, 910–918.

(73) Berger, O.; Edholm, O.; Jähnig, F. *Biophys. J.* **1997**, *72*, 2002–2013.

(74) Höltje, M.; Förster, T.; Brandt, B.; Engels, T.; von Rybinski, W.; Höltje, H.-D. *Biochim. Biophys. Acta* **2001**, *1511*, 156–167.

(75) Edholm, O.; Nagle, J. F. *Biophys. J.* **2005**, *89*, 1827–1832.

(76) Javanainen, M.; Melcrová, A.; Magarkar, A.; Jurkiewicz, P.; Hof, M.; Jungwirth, P.; Martinez-Seara, H. *Chem. Commun.* **2017**, *53*, 5380–5383.

(77) Antila, H. S.; M. Ferreira, T.; Ollila, O. H. S.; Miettinen, M. S. *J. Chem. Inf. Model.* **2021**, *61*, 938–949.